Applied Catalysis B: Environmental 185 (2016) 281–294

Contents lists available at ScienceDirect

Applied Catalysis B: Environmental

journal homepage: www.elsevier.com/locate/apcatb

Bimetallic Au–Cu, Au–Ni catalysts supported on MWCNTs for oxy-steam reforming of methanol

Pawel Mierczynski[a,*], Krasimir Vasilev[b], Agnieszka Mierczynska[c], Waldemar Maniukiewicz[a], Malgorzata I. Szynkowska[a], Tomasz P. Maniecki[a]

[a] Institute of General and Ecological Chemistry, Lodz University of Technology, Zeromskiego 116, 90-924 Lodz, Poland
[b] Mawson Institute, University of South Australia, Mawson Lakes, SA 5095, Adelaide, Australia
[c] The Australian Wine Research Institute, Waite Precinct, Hartley Grove cnr Paratoo Road, Urrbrae, Adelaide, SA 5064, Australia

ARTICLE INFO

Article history:
Received 7 September 2015
Received in revised form
21 November 2015
Accepted 27 November 2015
Available online 11 December 2015

Keywords:
Oxy-steam reforming of methanol
Au–Cu
Au–Ni
Bimetallic catalysts
Carbon nanotubes
Nanomaterial
Nanocatalyst

ABSTRACT

This paper interrogates for the first time the catalytic properties of bimetallic Au–Cu/MWCNTs and Au–Ni/MWCNTs catalysts in oxy-steam reforming of methanol. X-ray diffraction (XRD), specific surface area and porosity, scanning electron microscopy with X-ray microanalysis (SEM-EDS), thermo-gravimetric analysis, temperature programmed desorption of ammonia and X-ray photoelectron spectroscopy (XPS) were used to characterize the MWCNT supported catalysts. A significant impact of Au–Cu and Au–Ni alloy phases on the selectivity to hydrogen formation of the bimetallic catalysts in oxy-steam reforming of methanol was demonstrated. The Au–Cu/MWCNTs catalyst exhibited higher selectivity to hydrogen formation and lower selectivity to carbon monoxide formation. Whereas the introduction of copper, nickel and/or gold phase into MWCNTs facilitated thermal decomposition of the nanomaterial. The acidity data correlate well with the catalytic activity results. The spillover effect between copper (II) oxide and metallic gold or nickel (II) oxide and metallic gold was proven. Reactivity investigation on bimetallic 1%Au–20%Ni/MWCNTs catalyst used for oxy-steam reforming of methanol reaction confirmed the possibility of application of this system as a electrode material for fuel cell technology.

1. Introduction

Hydrogen can be obtained by catalytic reforming of methanol, partial oxidation of methanol or a combination of these two processes, termed oxy-steam reforming of methanol. Given the relatively mild conditions to conduct this process (P = 1 atm, T = 150–350 °C), it appears feasible to produce hydrogen directly at the place where it is needed. Production of hydrogen by oxy-steam reforming of methanol enables running the reaction in autothermal way, which is economically very advantageous. Hydrogen produced via oxy-steam reforming of methanol can be applied in fuel cells designed to power small mobile devices such as mobile phones, laptops, meteorological stations and any others low power devices. However, an outstanding challenge is obtaining pure hydrogen (clean of carbon monoxide) which can be used directly to power fuel cells. Supported catalysts, which are used in this reaction, undergo very fast deactivation, mainly due to their poisoning by carbon monoxide and overheating [1–3].

Typical catalysts used in methanol reforming are copper [1–5] and nickel [6–8] based system. Factors that affect the catalytic activity of copper or nickel supported catalysts are the dispersion of the metallic phase, the surface area and the particle size of copper or nickel species. An opportunity to improve the activity and selectivity of the copper or nickel supported catalyst is adding promoters, most often other metals such as Au [9–13], Ag [14], Pd [3,15]. It is now well documented that bimetallic supported catalysts show superior catalytic properties compared to monometallic catalysts. However, other factors such as particle size, support type and catalyst stability play major roles in this process [12].

An important consideration is selecting a suitable catalyst support. Typical catalyst carriers used in methanol reforming reactions are ZnO, Al_2O_3, CeO_2, SiO_2, Al_2O_3, ZnO–Al_2O_3, ZrO_2–Al_2O_3, CeO_2–Al_2O_3, CeO_2–ZrO_2, MCM-41, carbon black, ceramic slices etc. Carbon nanotubes (CNTs) have recently become an attractive

* Corresponding author. Fax: +61 48426313128.
E-mail addresses: pawel.mierczynski@p.lodz.pl (P. Mierczynski), krasimir.vasilev@unisa.edu.au (K. Vasilev), agnieszka.mierczynsaka-vasilev@awri.com.au (A. Mierczynska), waldemar.maniukiewicz@p.lodz.pl (W. Maniukiewicz), malgorzata.szynkowska@p.lodz.pl (M.I. Szynkowska), tomasz.maniecki@p.lodz.pl (T.P. Maniecki).

http://dx.doi.org/10.1016/j.apcatb.2015.11.047
0926-3373/

support material because of their extraordinary properties, which are beneficial in many applications. In particular, CNTs have high thermal and mechanical stability. Furthermore, CNTs have very high surface area, capacity to adsorb catalytically active nanoparticles inside the nanotubes and on their external wall, electron structure that supports conductivity and promotes "spillover" effect on the interface created by the active centers. Importantly, nanoparticles of an active phase introduced on the functional surface of the CNTs are easily accessible to the reactants [16]. In addition, many of the properties of carbon nanotubes can be enhanced when modified, functionalized or doped.

However, there are only a handful of published reports concerned with the use of carbon nanotubes as a catalytic support in reforming of methanol [17,18]. Specifically, there is no published study that explores the properties and performance of bimetallic catalysts supported on carbon nanotubes. In view of the extraordinary properties of CNTs and the urgent need for novel catalysts in methanol reforming, it is important to shed light on the potential of CNTs as a support in bimetallic systems.

In our previous work [3] we confirmed an alloy formation between Pd and Cu during activation process. We have proven that the alloy has a significant influence on the catalyst properties and especially on its selectivity. Based on these encouraging results we decided to carry out systematic studies focused on alloy formation between Au and Cu or Au and Ni on multi-walled carbon nanotubes (MWCNTs).

Specifically, the aim of this work was to elucidate the nature of interactions between gold and copper, and gold and nickel atoms, and their reactivity in oxy-steam reforming of methanol. Further the study aims to reveal the relationship between the surface composition of Au–Cu and Au–Ni bimetallic catalysts supported on CNTs with their catalytic behavior. In order to achieve these goals, monometallic Cu, Ni and bimetallic Au–Cu, Au–Ni supported catalysts were prepared and their physicochemical properties studied by specific surface area and porosity (BET), thermo-gravimetric analysis (TG), X-ray diffraction (XRD), temperature programmed reduction (TPR-H_2) and X-ray photoelectron spectroscopy (XPS). Catalytic activity tests in oxy-steam reforming of methanol were carried out using fixed bed quartz reactor under atmospheric pressure at two temperatures 200 and 300 °C, respectively.

2. Experimental

2.1. Catalysts preparation

Copper or nickel catalysts were prepared by wet aqueous impregnation. Metal phase of Cu or Ni was introduced on the multi-walled carbon nanotubes surface (MWCNTs—purchased from Sigma–Aldrich CAS:308068-56-6) by wet impregnation using aqueous solutions of copper nitrate or nickel nitrate. The supported catalysts were then dried for 2 h at 120 °C and calcined for 4 h in air at 350 °C.

Gold phase was introduced on monometallic copper or nickel catalyst surface by deposition–precipitation method described in Ref. [19]. In the first stage of preparation of the bimetallic supported catalysts, an aqueous solution of chloroauric acid was added into the solution containing suspended Cu/MWCNTs catalyst under vigorous stirring at 65 °C. In the next step, urea was used to achieve pH 8. The gold loading in the catalyst was 1 wt.%. After aging for two hours, the precipitate was filtered and washed with hot water until no chloride ions were detected using 0.1 M $AgNO_3$ solution. Then the resulting precipitate was dried overnight in air at 80 °C, and afterwards it was calcined at 180 °C for 4 h in air atmosphere. Copper and gold or nickel and gold loading were 20 wt.% and 1 wt.%, respectively. Monometallic gold (2%Au/MWCNTs) catalysts were also prepared by deposition–precipitation method described in Ref. [19]. Then the supported gold catalyst was dried overnight at 80 °C and calcined for 4 h in air at 180 °C.

2.2. Characterisation methods

The specific surface area and porosity of supports and catalysts were determined by the BET based on low temperature (77 K) nitrogen adsorption in a Micrometrics ASAP 2020 apparatus.

Thermo-gravimetric TG method, equipped with differential thermal analysis DTA device Derivatograpf Type: 34-27T (MOM BUDAPEST) was used for temperature programmed decomposition of nonmaterial's including multi-walled carbon nanotubes and mono- and bimetallic Au–Cu and Au–Ni catalysts in air atmosphere. The TG-DTA measurements were carried out applying sample weight about 50 mg, linear heating rate of 10 °C min^{-1}, temperature range from 25 up to 1000 °C. Such sample was used without any preliminary treatment.

TG-DTA-MS measurements for $AuCl_3 \cdot xH_2O$ were performed using Setaram SETSYS-16/18 device in air and reduced atmosphere (2% H_2–98% Ar). The TG-DTA-MS measurements were carried out with sample weight of ~10 mg, linear heating rate of 10 °C min^{-1}, and temperature range from 25 up to 1000 °C.

The TPR-H_2 measurements were carried out in an automatic TPR system AMI-1 in the temperature range of 25–900 °C with a linear heating rate of 10 °C min^{-1}. Samples (weight about 0.1 g) were reduced in hydrogen stream (5% H_2–95% Ar) with a volumetric flow rate of 40 cm^3 min^{-1}. Hydrogen consumption was followed by a thermal conductivity detector.

The TPD-NH_3 measurements were carried out in a quartz reactor using NH_3 as a probe molecule. The NH_3 was adsorbed on the samples at 50 °C for 30 min after purification of catalyst surface in flowing He at 600 °C for 60 min. The temperature programmed desorption of NH_3 was carried out in the temperature range 100–600 °C using a linear growth of temperature (25 °C min^{-1}) and a thermal-conductivity detector, after removing physisorbed ammonia from the sample surface.

Powder X-ray diffractograms were recorded on a PAN analytical Pro MPD using Cu Kα radiation (λ = 154.05 pm) in 2θ range of 5–90°.

The SEM measurements were performed using a S-4700 scanning electron microscope HITACHI (Japan), equipped with an energy dispersive spectrometer EDS (Thermo Noran, USA). Images were recorded at several magnifications using secondary electron or BSE detector. The accelerating voltage was 25 kV.

The XPS spectra were recorded on a Specs SAGE XPS spectrometer using Mg Kα radiation source (hν = 1253.6 eV) operating at 10 kV and 20 mA. The elements present on the sample surface were identified from a survey spectrum recorded over the energy range 0–1000 eV at a pass energy of 100 eV and a step of spectra acquisition of 0.5 eV. The areas under selected photoelectron peaks in the spectrum were used to calculate the percentage of atomic concentrations. High resolution (step of spectra acquisition of 0.1 eV) spectra were then recorded for pertinent photoelectron peaks at a pass energy of 20 eV to identify the chemical state of each element. All the binding energies (BEs) were referenced to the C1s neutral carbon peak at 285 eV, to compensate for the effect of surface charging. The analysis area was circular with a diameter of 0.7 mm. The processing and curve-fitting of the high-resolution spectra was performed using CasaXPS software.

2.3. Catalytic tests

Oxy-steam reforming of methanol (OSRM) was performed using a flow quartz reactor under atmospheric pressure. The reaction was carried out at two temperatures 200 and 300 °C, respectively. HPLC grade methanol (Aldrich, water ~0.03 wt.%) was used.

The catalyst load was 0.1 g and the stream composition was: $H_2O/CH_3OH/O_2 = 1/1/0.4$ (molar ratio) and the GHSV was 26700 h^{-1} (calculated at ambient temperature and under atmospheric pressure). The total flow-rate was kept at 31.5 ml/min and the Ar was used as the balance gas (the methanol content in the reaction mixture was 6%). The steady-state activity measurements at each temperature were taken after at least 2 h in the stream. The analysis of the reaction organic products (methanol, methane, methyl formate, dimethyl ether (DME), formaldehyde) was carried out by an on-line gas chromatograph equipped with FID detector and 10% Carbowax 1500 on Graphpac column. The CO, CH_4 and CO_2 concentrations were followed by a GC chromatograph equipped with TCD detector (150 °C, 60 mA), and Carbopshere 60/80 (50 °C) column. The hydrogen concentration was measured by a GC chromatograph equipped with TCD detector (120 °C, 60 mA) and molecular sieve 5a (120 °C) column. Material balances on carbon were calculated to verify the obtained results. The selectivity towards the formation of hydrogen, carbon monoxide or carbon dioxide in OSRM was calculated using Eqs. (1)–(3) and the conversion of methanol using Eq. (4):

$$S_{H_2}(\%) = \frac{(nH_{2-out})}{\sum \text{products of the reaction}} \times 100 \quad (1)$$

$$S_{CO}(\%) = \frac{(nCO_{out})}{\sum \text{products of the reaction}} \times 100 \quad (2)$$

$$S_{CO_2}(\%) = \frac{(nCO_{2-out})}{\sum \text{products of the reaction}} \times 100 \quad (3)$$

where, nCH_3OH and nH_2 is the molar flow rate of CH_3OH and H_2, respectively.

$$\text{Conv.}_{CH_3OH} = \frac{n_1{}^{in}CH_3OH - n_2{}^{out}CH_3OH}{n_1{}^{in}CH_3OH} \times 100 \quad (4)$$

where nH_{2-out} H_2—molar flow rate of H_2 feed out, nCO_{2-out}—molar flow rate of CO_2 feed out, nCO_{out}—molar flow rate of CO feed out, $n_1{}^{in}$ CH_3OH, $n_2{}^{out}$ CH_3OH—molar flow rate of CH_3OH feed in and feed out, respectively. Methane, formaldehyde, dimethyl ether and methyl formate formation were not observed. Only carbon monoxide was formed as intermediates during the reaction.

3. Results and discussion

3.1. Thermo-gravimetric TG analysis

The thermal stabilities of multi-walled carbon nanotubes and catalysts were investigated in order to determine the influence of metal addition on the susceptibility of MWCNTs to oxidation and confirm the stability of mono- and bimetallic supported catalysts under the reaction conditions. The results of the thermal decomposition measurements carried out for all systems are presented in Fig. 1A and B, respectively.

The TG measurements showed that MWCNTs decompose in two stages (see Fig. 1A). The process of water removal and impurities takes place in the temperature range 30–200 °C. This is evident by the changes in the TG and DTG curves associated with the endothermic DTA peak situated in the temperature range 30–200 °C. The second stage is associated with the oxidation of multi-walled carbon nanotubes [20] directly to carbon dioxide. This can be seen in the temperature range 520–980 °C. This is consistent with Mahajan et al. [20] who studied the thermal decomposition of MWCNTs under different atmospheres and showed that multi-walled carbon nanotubes are stable in air up to 420 °C. The authors did not observe any changes on the TG-DTA curves during the analysis under non isothermal conditions.

The same decomposition stages were also observed in the case of mono- and bimetallic catalysts. Notably the stages associated with the oxidation of carbon nanotubes were seen at different decomposition temperature depending on the catalyst. The observed differences are related to the catalytic effect of the metal oxide or metallic phase, the presence of which facilitates the oxidation process of carbon nanotubes. The studied catalysts were not degraded fully. The residue was comprised of NiO or CuO or/and metallic gold phase.

It should be stressed that complete decomposition of the mono- and bimetallic catalysts supported on CNTs occurs at a lower temperature compared to the decomposition temperature of carbon nanotubes. In the case of monometallic gold catalysts, the MWCNTs decompose in the temperature range 520–950 °C. The introduction of copper or nickel into the nanomaterial results in further decrease of the initial decomposition temperature. The TG curves of monometallic copper and nickel supported catalysts showed that multi-walled carbon nanotubes start to decompose at 470 and 450 °C, respectively. The thermal decomposition process of 20%Ni/MWCNTs catalysts ends at 780 °C, whereas for the 20%Cu/MWCNTs supported catalyst this process ends at 760 °C. Promotion of monometallic catalysts by gold caused a further decrease of the initial decomposition temperature of the carbon nanotubes to 380 °C for the gold–nickel supported catalyst and to 370 °C for the gold–copper catalyst, respectively. No significant effect of gold promotion on the final decomposition temperature of the monometallic Cu and Ni catalysts was observed. The TG, DTG and DTA data confirmed the results obtained.

Yang and Liao [21] prepared Cu/ZnO-CNTs by chemical reduction and wet impregnation, and studied their thermal decomposition to determine the true metal loading and to analyze the thermal properties of the support carbon nanotubes. The authors claimed that commercial CNTs without pre-treatment, with impurities level of about 3–5%, had cracking temperature at 570 °C, whereas pre-treated CNTs had higher cracking temperature (645 °C) as a results of impurities elimination. Furthermore, these workers found that functional groups introduced during the chemical treatment of CNTs reduced the hydrophobicity of CNTs, resulting in an enhanced affinity of the metal precursors on the surfaces.

Collectively, the thermal analysis results point that the prepared supported monometallic Au, Cu and Ni catalysts are stable in air atmosphere up to temperature of 520, 470 and 450 °C, respectively. The bimetallic Au–Cu and Au–Ni supported catalysts are stable in the same atmosphere up to 380 and 370 °C, respectively. These results clearly indicate that the catalytic systems are stable in the temperature range used in oxy-steam reforming of methanol i.e., at 200 and 300 °C, respectively. These results also shown that addition of metals oxides facilitate the thermal decomposition of multi-walled carbon nanotubes.

3.2. The specific surface area of the catalytic materials

The specific values of the catalyst surface area (BET), monolayer capacity and average pore radius for MWCNTs, mono- and bimetallic supported catalysts are presented in Table 1. BET measurements show that the highest specific surface areas have bimetallic Au–Ni supported catalysts. The introduction of a metallic gold phase into Cu/MWCNTs causes decrease in specific surface area. The specific surface area is reduced from 290 $m^2\,g^{-1}$ for copper supported catalyst to 272 $m^2\,g^{-1}$ for bimetallic Au–Cu system calcined at 180 °C. The same trend was observed after introduction of higher quantity of copper oxide phase. This may be caused by pores blocking of the support by the copper oxide or metallic gold phase. A comparison of the specific surface area of Cu/MWCNTs and Ni/MWCNTs catalysts suggests that the extent of pore blockage in the Ni/MWCNTs

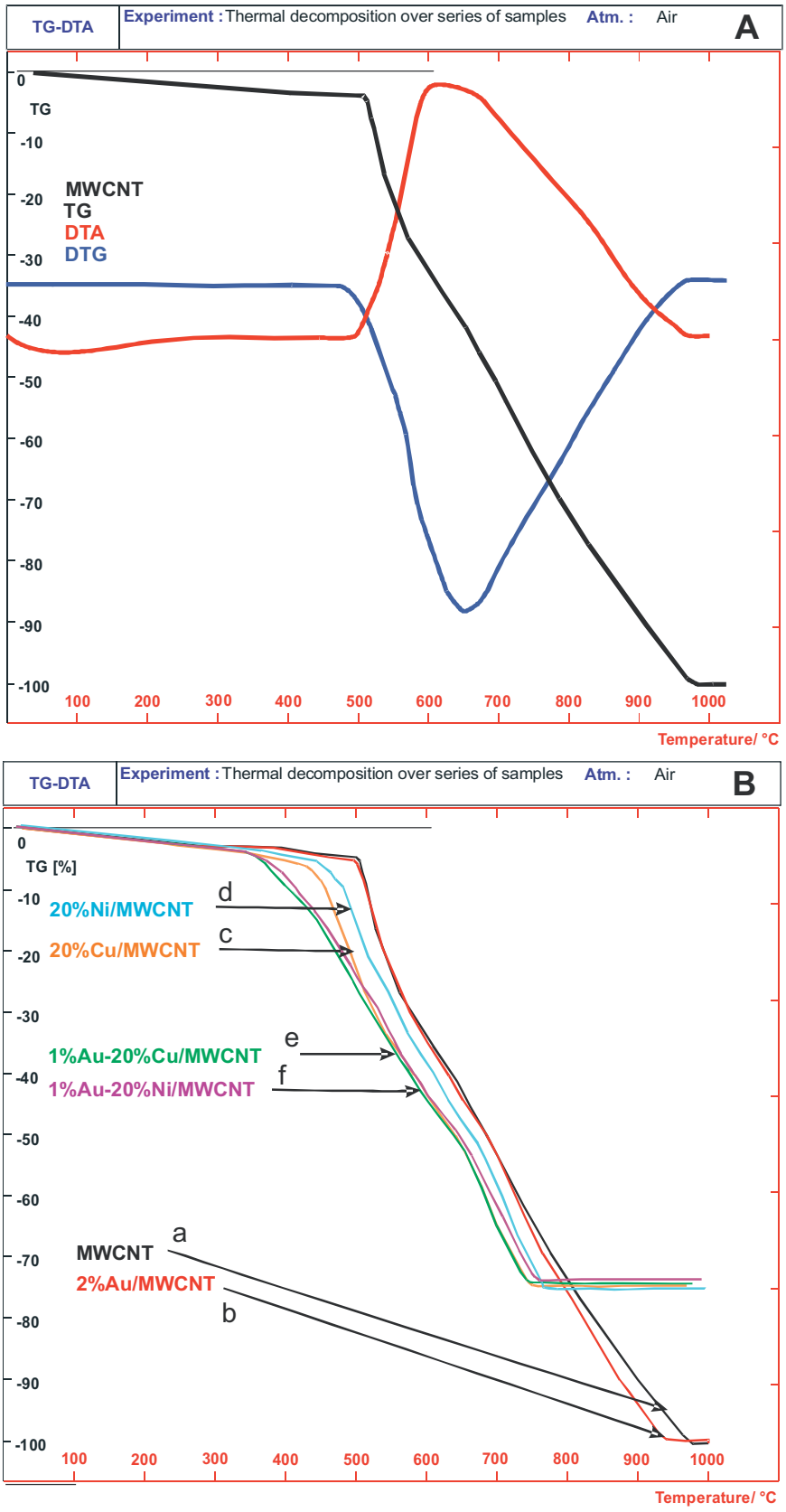

Fig. 1. (A) TG, DTA and DTG curves for multiwalled carbon nanotubes, (B) (a) multiwalled carbon nanotubes, monometallic supported catalysts (b) 2%Au/MWCNTs (c) 20%Cu/MWCNTs (d) 20%Ni/MWCNTs and bimetallic catalysts (e) 1%Au–20%Cu/MWCNTs (f) 1%Au–20%Ni/MWCNTs obtained during temperature programmed decomposition process performed in air atmosphere.

Table 1
Results of BET surface area, total pore volume and average pore radius.

Material/$T_{calc.}$	BET surface area [m^2/g]	Total pore volume [cm^3/g]	Average pore radius [nm]
MWCNTs	282	2.13	12.0
1%Au–20%Cu/MWCNTs/180 °C	272	0.938	5.90
1%Au–20%Ni/MWCNTs/180 °C	311	0.861	4.84
5%Cu/MWCNTs/350 °C	290	1.36	8.13
20%Ni/MWCNTs/350 °C	271	1.28	8.11
20%Cu/MWCNTs/350 °C	290	1.36	8.13

is higher than that in the Cu/MWCNTs system. Table 1 shows that with increasing of the metal content in the catalytic material the total pore volume decreases in all systems. Whereas, completely different behaviour was observed in average pore radius.

Abbaslou et al. [22] investigated the BET surface area of Fe/CNT catalysts and also observed decrease of the value of specific surface area after iron impregnation This was explained by blockage of the support pores.

3.3. Reduction behavior

The reducibility of the MWCNTs supported catalysts was studied to determine the influence of the activation process (reduction in a 5%H_2–95%Ar mixture) on their reactivity in oxy-steam reforming of methanol and the interaction between active phase component and support. The reduction measurements carried out for pure MWCNTs, mono- (Au, Cu Ni) and bimetallic supported catalysts (Au–Cu and Au–Ni) are given in Fig. 2. The reduction measurement showed that pure MWCNTs were not reduced in the temperature range 25–900 °C.

In the case of monometallic gold supported catalysts only one wide peak located in the temperature range of 360–700 °C was visible, associated with desorption of the hydrogen chloride from the carbon material. The desorbing hydrogen chloride originated from the decomposition of the gold chloride formed during the calcination process of the catalyst system. During the calcination step (performed at 180 °C) chlorine was not completely removed from the system (see Supplementary information S1). In addition, the observed effect is not connected with the $HAuCl_4$ reduction because its reduction takes place at lower temperature (up to 250 °C) [23].

To better understand the TPR, results TG-DTA-MS measurements of gold (III) chloride in air and reductive atmosphere were performed and are shown in Figs. 3 and 4, respectively.

Thermal decomposition of $AuCl_3 \cdot xH_2O$ in air atmosphere is shown in Fig. 3. Gravimetric analysis and MS show three stages of $AuCl_3$ decomposition. The first stage relates to the removal of moisture from the unbound coordination sphere of the cation. This process occurs in a temperature range of 50–200 °C. The second stage is related to the decomposition of anhydrous gold (III) chloride to form the gold (I) chloride. This stage is accompanied by the simultaneous evolution of chlorine ($m/z = 70$) and hydrogen chloride ($m/z = 36$). This process occurs in a temperature range of 200–270 °C. The third stage is assigned to the decomposition of gold (I) chloride. This step is accompanied by desorption of HCl ($m/z = 36$) and Cl_2 ($m/z = 70$). This process occurs in a temperature range of 270–350 °C. Visible chlorine evolution can be explained by disassociate decomposition, whereas formation of hydrogen chloride gas can be explained by a metastable oxychloride structure according to the following scheme [24]:

$$AuCl_3 + xH_2O \rightarrow AuCl_{(3-y)}(OH)_y + yHCl + (x-y)H_2O$$

$$AuCl_{(3-y)}(OH)_y + 0.5yO_2 \rightarrow AuCl_{3-2y}O_{2y} + yHCl$$

This reasoning is not reflected in the results from the thermal analysis. The oxygen absorption was not observed in the decomposition temperature range. Finally, the decomposition process can be exemplified by the following scheme:

$$AuCl_3 \rightarrow AuCl \rightarrow Au$$

The quantitative analysis of the thermal decomposition of $AuCl_3 \cdot xH_2O$ was based on the theoretical and real weight loss (theoretical weight loss [%] = 35.1, real weight loss [%] = 32.6). Attention should be drawn to the compatibility of the theoretical values with experimental data, which on supports our data interpretation and confirms that the investigated compounds are of satisfactory purity.

The decomposition process of $AuCl_3 \cdot xH_2O$ in an atmosphere of 2% H_2–98% Ar is presented in Fig. 4. TG, DTG, DTA curves and MS profiles of the concentration of hydrogen, water, hydrogen chloride and chlorine are given in the figure. The decomposition of hydrated gold (III) chloride takes place in the temperature range of 25–360 °C. Direct decomposition of $AuCl_3 \cdot xH_2O$ in a reductive atmosphere appears to be preceded by partial dehydration of gold (III) chloride and is described by the following equations:

$$AuCl_3 \cdot xH_2O \rightarrow AuCl_3 + xH_2O$$

$$AuCl_3 + H_2 \rightarrow AuCl + 2HCl(175–260\,^\circ C)$$

$$AuCl + 1/2H_2 \rightarrow Au + HCl(260–360\,^\circ C)$$

The reduction of gold (I) chloride in a mixture of 2%H_2–98%Ar is accompanied by the release of relatively small amounts of chlorine (see Fig. 4), which indicates that part of the reductive chloride phase undergoes self-degradation according to the equations:

$$AuCl_3 \rightarrow AuCl + Cl_2$$

$$AuCl \rightarrow Au + 1/2Cl_2$$

Collectively, the decomposition processes of $AuCl_3 \cdot xH_2O$ performed in air or reductive atmosphere provide evidence that this compound is completely decomposed at temperatures of up to 360 °C and indicate that the observed effect on the TPR-H_2 recorded for 2%Au/MWCNTs is not connected with the $AuCl_3$ reduction process.

Additionally, the wide peak observed on the TPR-H_2 profile in the temperature range of 360–700 °C is connected with the carbon nanotubes methanation process. Methanation occurs also in the case of the reduction process carried out for copper supported catalysts, starting at 390 °C and ending at about 800 °C [25–27].

Both mono and bimetallic supported multi-walled carbon nanotubes catalysts showed reduction stages on the TPR profile. In the case of copper supported catalysts three stages can be easily observed on the TPR profile recorded for this system (see Fig. 2A). The first two partially resolved profiles were visible at about 220 and 300 °C, respectively. These reduction stages are attributed to the two-step reduction of the copper oxide (II) via the intermediate Cu_2O. In the literature data one can find another explanation of the observed two-step reduction process of CuO. These two effects visible on the TPR curve are also assigned to the reduction process of small and large crystallite size of copper (II) oxide [21,28,29]. The

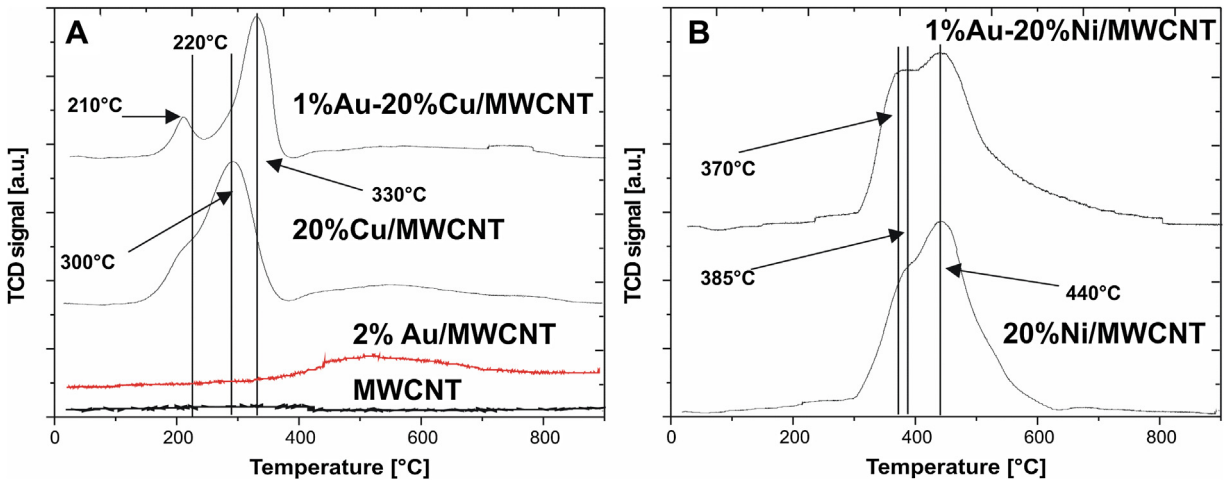

Fig. 2. TPR profile of (A) multi-walled carbon nanotubes, monometallic gold catalyst after calcination in air for 4 h at 180 °C, monometallic copper catalyst after calcination in air for 4 h at 350 °C and bimetallic Au–Cu/MWCNTs after calcination in air for 4 h at 180 °C and (B) for monometallic nickel catalyst after calcination in air for 4 h at 350 °C and bimetallic Au–Ni/MWCNTs catalysts after calcination in air for 4 h at 180 °C.

next peak located in the temperature range 390–800 °C is assigned to the methanation process of the MWCNTs which was visible in the same temperature range of the reduction process as in the case of the gold catalyst. The reduction mechanism of copper (II) oxide running through an intermediate stage Cu_2O [30,31] is confirmed by the in situ XRD data obtained during the reduction process carried out in a 5%H_2–95%Ar mixture for copper 20%Cu/MWCNTs catalyst [27].

The reduction behaviour of copper catalysts supported on MWCNTs were studied by Song and Jiang [32]. On the TPR profile recorded during the reduction process of copper catalysts only one hydrogen consumption peak in the range of 100–300 °C was visible for all studied samples, which corresponds to the reduction of CuO. The reduction studies also confirmed that pristine MWCNTs are not reducible in the investigated temperature range. After performing reducibility studies, the authors noted that increasing in the MWCNTs defect density caused lowering of the maximum of the hydrogen consumption peak. The high defects density in the MWCNTs facilitated the reduction of CuO species in comparison to highly perfect graphitize structures. The defects of MWCNTs could promote electron transfer during the reduction process which directly destabilizes Cu—O bonds and thereby facilities the reduction of CuO to metallic copper [33].

On the other hand nickel supported catalyst showed three stages on the TPR profile. The first two partially resolved reduction profiles which were attributed to the reduction of two kinds of NiO surface species weakly and strongly interacting with carbon situated at 385 and 440 °C, respectively [34] (see Fig. 2B). The third peak located in the high temperature range, which is partially visible in temperature range 600–800 °C is assigned to the methanation process of the MWCNTs. Zhou et al. [35] studied the reduction behavior of Ni catalyst supported on MWCNTs and observed two reduction peaks. The first peak situated at 300–370 °C temperature range was attributed to H_2 consumption connected with the reduction of superficial NiO species poorly or not interacting with the carrier. The second broad TPR peak situated around 420–560 °C was assigned to the reduction of highly dispersed NiO strongly interacting with the MWCNTs. The authors also claimed that increasing of metal content in the catalytic systems increases the intensity of the second peak assigned to NiO strongly interacting with support.

Introduction of gold to the monometallic copper catalyst caused changes of the reduction behavior of the Cu catalyst (see Fig. 2A). In the case of gold–copper catalyst four partially resolved reduction stages are visible on the TPR profile. The first stage with maximum hydrogen consumption located at about 210 °C is assigned to the CuO species reduction to Cu_2O. The second one with the maximum of hydrogen consumption peak situated at 300 °C is attributed to the Cu_2O species reduction to metallic copper. It is worth notice that the first peak is shifted towards lower temperature range compared to the reduction stage observed in the case of Cu/MWCNTs catalyst. This confirms the spillover effect, which take place between copper (II) oxide and metallic gold phase for this system. The third reduction effect with the maximum of hydrogen consumption peak located at about 330 °C is assigned to the copper oxychlorides species ($Cu_2(OH)_3Cl$) reduction. It is worth to note that the third peak is shifted in comparison to the second reduction peak observed in the case of copper catalysts. This can be explained by the fact that the copper (II) oxide is in direct contact with the oxychlorides present on the surface of the carrier. These oxychlorides species may stabilize the CuO species on the MWCNTs surface.

During the preparation step of the bimetallic Au–Cu catalyst $Cu_2(OH)_3Cl$ are formed. In the first step copper (II) chloride is formed from the chloride ions coming from chloroauric acid, which was introduced during the preparation step of bimetallic catalyst, by deposition–precipitation method using urea as a precipitation agent. Copper (II) oxychlorides are formed on the surface of the MWCNTs as a result of hydrolysis of a $CuCl_2$ solution even at pH 4–7 according to the following equation [36]:

$$2CuCl_2 + 3OH^- \rightarrow Cu_2(OH)_3Cl + 3Cl^-$$

Hydroxyl ions resulting from urea hydrolysis react with copper (II) chloride and in the final stage form the $Cu_2(OH)_3Cl$ species [37]. The resulting connections of Cu—OH—Cl formed during the preparation of the catalyst are harder to reduce in comparison to the copper oxide species.

The fourth reduction effect observed on the TPR-H_2 profile is located in the temperature range 390–800 and is assigned to the same effect, which was visible at the same temperature range as for 20%Cu/MWCNTs system.

The TPR-H_2 profile recorded for nickel-gold doped MWCNTs supported catalyst is given in Fig. 2B and shows that promotion of nickel catalyst by gold changes its reducibility. Two unresolved reduction peaks co-located with the maximum of hydrogen consumption at about 370 and 440 °C in the reduction curve of Au–Ni bimetallic catalyst are also shown and are associated with the reduction of the same species as in the case of nickel catalyst. However, the relative proportions of the corresponding effects have been changed. Interestingly, the first reduction peak increased in

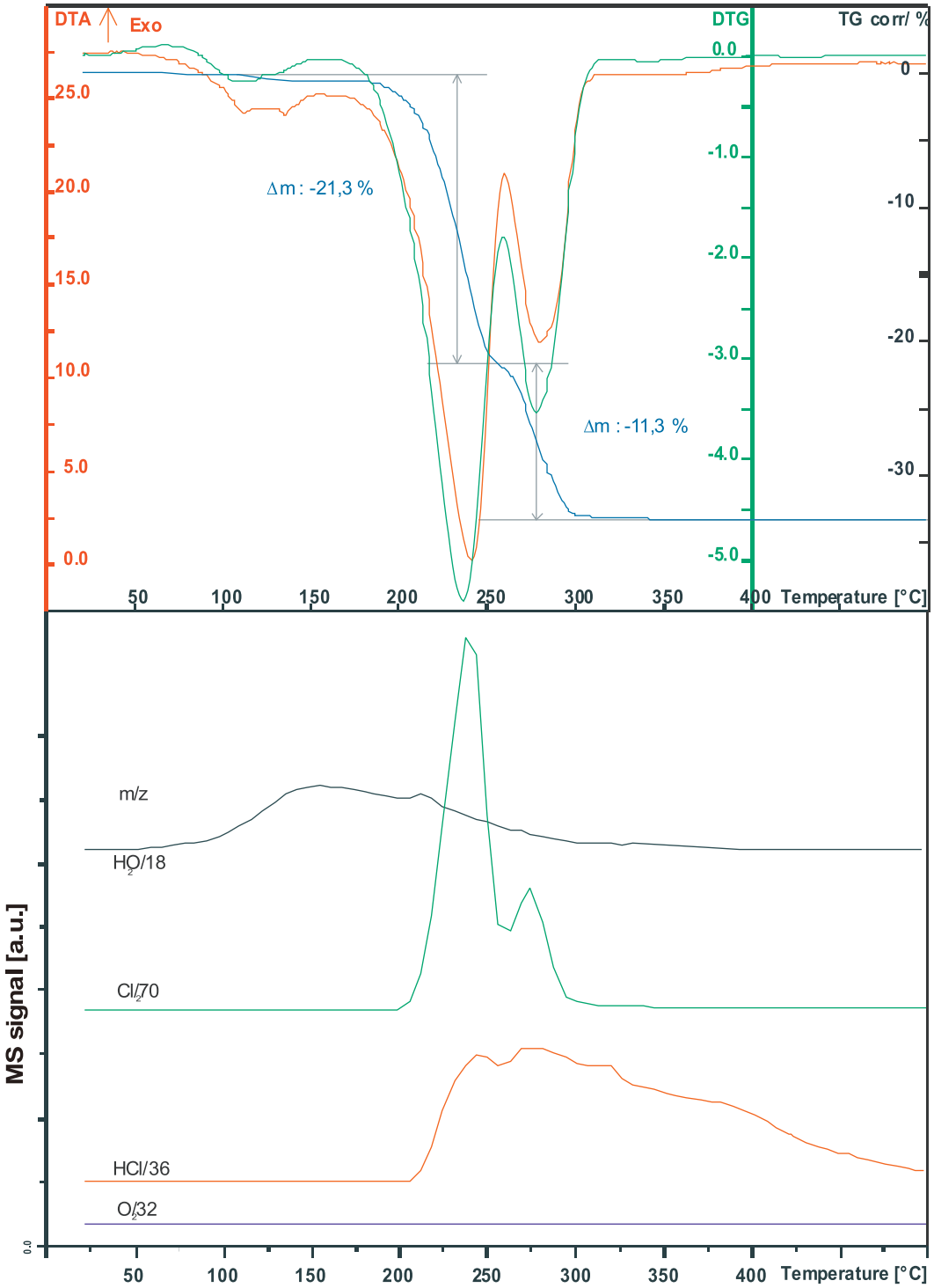

Fig. 3. TG, DTG, DTA and MS curves for thermal decomposition of $AuCl_3 \cdot xH_2O$ in air atmosphere.

intensity and shifted to lower temperature range as compared to the reducing peak observed for unpromoted catalysts. This result suggests that addition of gold to nickel catalysts facilitates the reduction of nickel oxide, strongly interacting with the carrier because of spillover phenomenon. It is well documented in the literature that adsorbed hydrogen on gold nanoparticles dissociates to atomic hydrogen, which flows down to the adjacent metal oxide. Additionally, the spillover effect between metallic gold and nickel oxide confirm the presence of these phases adjacent to each other. It is also reported that the process of reduction of copper or nickel catalyst is facilitated as a result of gold promotion and this is explained by spillover phenomenon between copper oxide and metallic gold, or nickel oxide and metallic gold [38–42]. This effect is manifested by the shifting of the reduction stages attributed to copper oxide or nickel oxide species reduction.

In addition, the shape of the second reduction peak observed on the TPR-H_2 profile may suggest, that the same effect which is ending at 800 °C, should be also assigned to the methanation process of MWCNTs as is the case for the nickel catalyst.

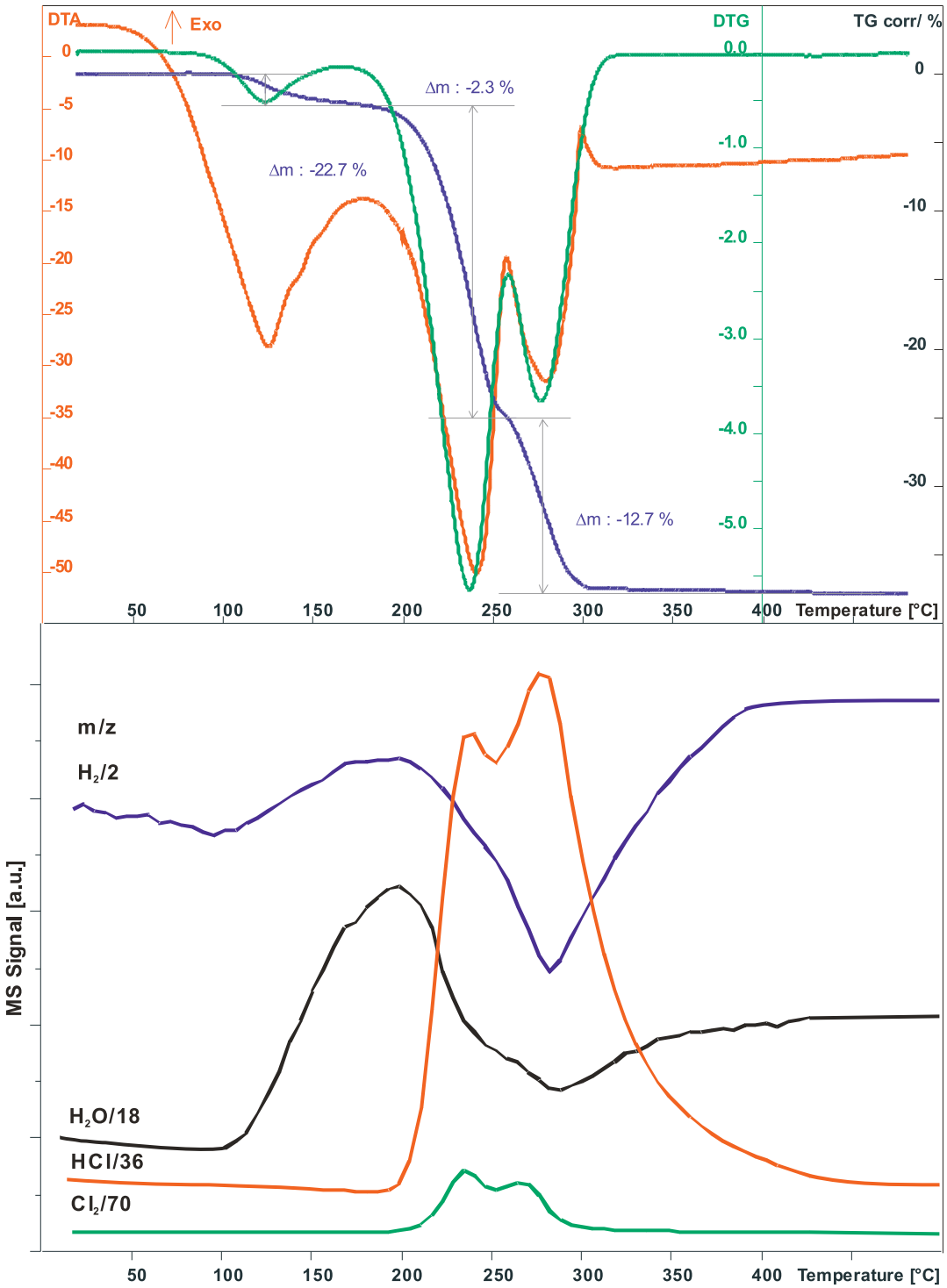

Fig. 4. TG, DTG, DTA and MS curves for thermal decomposition of $AuCl_3 \cdot xH_2O$ in a stream of 2% H_2–98% Ar.

3.4. The effect of gold on the phase composition of bimetallic catalysts

In order to examine the phase composition and explain the interaction between gold and copper or nickel, XRD studies of MWCNTs, mono and bimetallic catalysts were carried out. The results of the phase composition studies obtained for MWCNTs, mono and bimetallic supported catalysts reduced at 300 or 500 °C are given in Fig. 5. The diffraction curve of pure MWCNTs is shown in Fig. 5A. On the diffraction pattern of MWCNTs one can see only reflexes assigned to graphite-like phase. The XRD diffraction curve of monometallic gold catalyst show diffraction peaks that stem from a graphite-like phase corresponding to the MWCNTs and a metallic gold phase. X-ray reflections at $2\theta^\circ = 37.96^\circ$ (100%—peak (1 1 1)) and 44.38° (45%—peak (2 0 0)) correspond to metallic gold phase. XRD pattern of Cu/MWCNTs supported catalysts shows only diffraction peaks attributed to metallic copper and graphite like phases. Similarly, the presence of metallic nickel and graphite like phases were confirmed in the diffraction pattern of the nickel supported catalyst [21].

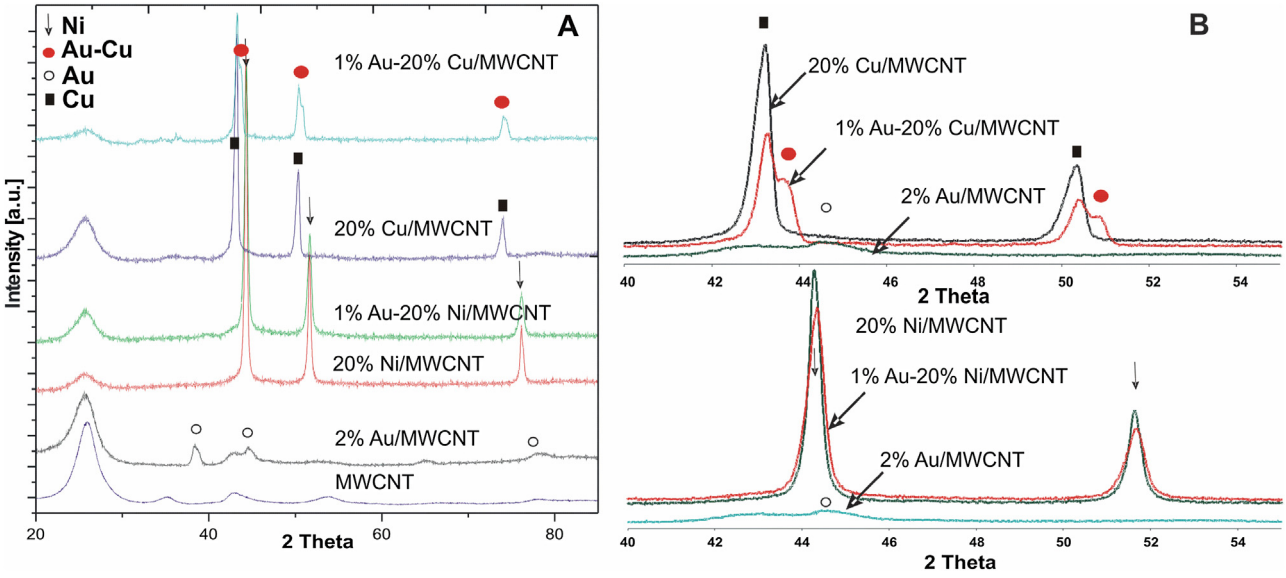

Fig. 5. (A) XRD patterns of MWCNTs, monometallic Au/MWCNTs catalyst being after calcination in air for 4 h at 180 °C, Cu and Au–Cu supported catalysts reduced in 5%H_2–95%Ar at 300 °C and monometallic Ni and Au–Ni supported catalysts reduced in 5%H_2–95%Ar mixture at 500 °C, (B) diffraction curves of monometallic Au, Cu, and bimetallic Au–Cu and Au–Ni catalysts in the range of 2θ° (40–55°).

Zhou et al. [35] investigated the phase composition of nickel catalysts supported on CNTs. They also observed the same crystallite phases corresponding to graphite-like tube-wall of the CNTs (confirmed by the diffraction peak positioned at 26.5°) and NiO and metallic Ni species depending on the catalyst treatment. Five composite materials consisting of 50 wt.% MO*x*/CNT (M: Co, Mn, Fe, Cu, Ni) were synthesized and characterized by XRD technique in Ref. [43]. The phase composition studies of these composite materials confirmed the presence of carbon CNTs and metal oxides corresponding to the particular catalysts composition.

The XRD pattern of reduced 1%Au–20%Cu/MWCNTs supported catalyst show diffraction peaks stemming from graphite like phase, metallic copper and an alloy Au–Cu phases. Diffraction peaks attributed to the alloy phase are visible at 2θ° = 43.75 and 51.00°. Alloying of copper and gold is further confirmed by the fact that the observed diffraction peak, originating from the alloy phase at 2θ = 43.75, is situated between the peak (1 1 1) of Cu and the peak (2 0 0) of gold phase (see Fig. 5B). The explanation of this result is the Au–Cu alloy formation which has a strongly oriented crystallites towards the peak coming from gold phase (2 0 0) [34].

However, in the case of 1%Au–20%Ni/MWCNTs catalysts, the only diffraction phases observed in the XRD curve were metallic nickel and graphite like phases. The lack of the reflexes coming from the metallic gold phase on the diffraction pattern recorded for bimetallic catalyst Au–Ni/MWCNTs confirms alloying process occurring between nickel and gold. The appearance of Au–Cu alloy phase in the diffraction pattern of bimetallic gold–copper supported catalyst and the lack of the gold phase in XRD curve in the case of gold-nickel catalyst confirms the interaction between these components, already found by the reduction studies.

In our previous work, [9] we studied the interaction between copper oxide and gold using XRD technique. Temperature programmed in situ XRD reduction measurements for Au–Cu reference material, with the weight ratio Au/Cu = 1:4 wt.% were carried out in a gas mixture of 5% H_2–95% Ar. The XRD patterns were collected in the temperature range from 50 to 800 °C for the reference sample in 5% H_2–95% Ar reductive mixture which was calcined beforehand for 4 h in air at 400 °C. The phase composition studies confirmed that the formation of alloy between metallic copper and gold phases starts from 300 °C. These findings correlate well with the results obtained for the bimetallic Au–Cu catalysts supported on multi-walled carbon nanotubes (see Fig. 5).

Analogous measurements in a 5% H_2–95% Ar gas mixture in the temperature range 25–880 °C over an Au–Ni reference material with the weight ratio Au/Ni = 1:4 wt.% were also carried out in our previous work [34] and an alloy formation Au–Ni was confirmed at 500 °C. The XRD in situ studies performed for reference material showed that in the temperature range 500–880 °C the Ni–Au alloy is formed which is manifested by the shift of the corresponding reflexes attributed to the Au and Ni phases. In the final reduction temperature at 880 °C only XRD diffraction peaks assigned to an alloy Ni–Au phase were visible. It is worth noting that in the XRD curve recorded for the reference material at 500 °C the shift of the reflexes assigned to Ni and Au metallic phases was insignificant.

In this work, we also confirmed the Au–Ni alloy formation for bimetallic Au–Ni/MWCNTs catalysts after reduction at 500 °C. The shift of the reflexes coming from the metallic nickel phase was not observed and also diffraction reflexes originating from the metallic gold phase were not visible on the diffraction curve. The above findings for reference material and bimetallic Au–Ni/MWCNTs catalysts and the spillover effects occurring between Au and NiO confirmed the alloy Au–Ni formation.

Additionally, phase composition studies for mono- and bimetallic supported catalysts after reduction and reaction were also studied (data not shown in the work). The analysis of the diffraction curves obtained for all of the samples confirmed the occurrence of the same phases for all catalysts which were detected for catalysts only after reduction.

Based on the TPR and XRD results, we can conclude that activation of Au–Cu/MWCNTs system at 300 °C and Au–Ni/MWCNTs at 500 °C in a reducing mixture causes alloy formation. It should be taken into consideration, that alloying causes changes in the catalytic properties of the active phase and may increase the catalytic activity and selectivity of the catalytic systems in oxy-steam reforming of methanol.

3.5. Interaction between the active phase components

Interaction between active phase component and the nature of the active species was investigated by XPS. The high resolution

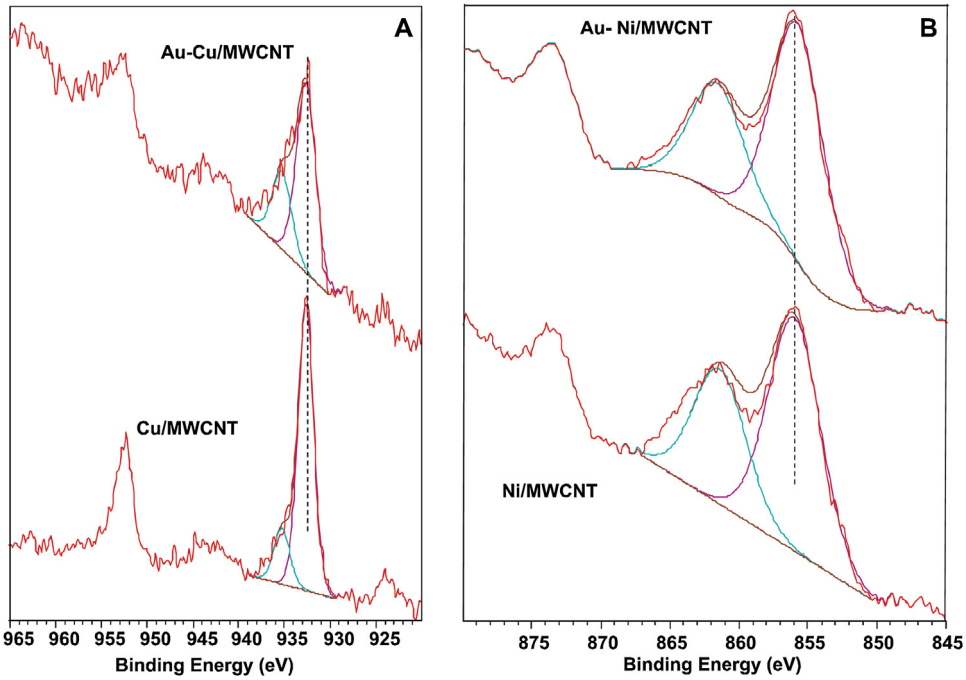

Fig. 6. (A) Cu 2p XPS spectra of 20%Cu/MWCNTs and 1%Au–20%Cu/MWCNTs for reduced catalysts in 5%H_2–95%Ar at 300 °C (B) Ni 2p XPS spectra of 20%Ni/MWCNTs and 1%Au–20%Ni/MWCNTs for reduced catalysts in 5%H_2–95%Ar at 500 °C.

spectra of reduced mono- and bimetallic supported catalyst collected in the respective binding energy range are shown in Fig. 6. The high resolution spectra of monometallic copper and gold doped copper supported catalysts after reduction are shown in Fig. 6A. The XPS high resolution spectra of the binding energies between 920 eV and 965 eV shows several characteristic peaks. The peak at about 933 eV includes Cu^{2+} species (933.5 eV) (Cu $2p_{3/2}$), metallic Cu° (932.7 eV) and Cu^{+} (932.4 eV). The peaks at about 943 eV and 963 eV are characteristic only for Cu^{2+} species [3].

The XPS spectra of copper promoted by gold catalysts showed a shift of the component assigned to metallic copper towards lower binding energy of approximately 0.07 eV with respect to the copper catalyst. This result confirmed the Au–Cu alloy formation during the activation process in a mixture of 5%H_2–95%Ar and is supported by the XRD data presented above.

Analogous measurements were also performed for nickel and gold–nickel supported catalysts and the results are given n Fig. 6B. The XPS high resolution spectra of the binding energies between 845 eV and 880 eV shows several characteristic peaks. The results for both catalysts showed shifts of the peak related to metallic nickel species in the case of bimetallic system towards lower energy of approximately 0.17 eV in comparison to Ni/MWCNTs system. This is evidence of alloying process occurring between metallic gold and nickel. These results are in good agreement with the measurements obtained by other researchers [44] and the XRD measurements performed in this work for bimetallic supported catalyst. For instance, Yang et al. [45] studied the formation of Ni–Au surface alloy at different annealing temperatures using XPS technique. They observed also the shift of the Ni $2p_{3/2}$ peak towards lower binding energy which was explained by the formation of the alloy.

3.6. Morphology studies of mono and bimetallic supported catalysts using SEM-EDS

A scanning electron microscope, equipped with an energy dispersive spectrometer EDS was employed to characterize the morphology and determine the elemental composition of the surface of the bimetallic catalytic systems. The results of the SEM-EDS measurements of bimetallic Au–Cu and Au–Ni supported catalysts after calcination at 180 °C are given in Fig. 7a and b, respectively. The magnification was 5000 in the case of bimetallic Au–Cu catalyst and 30000 in the case of bimetallic Au–Ni system.

The analysis of the surface composition of bimetallic catalysts showed the presence of copper, nickel, gold and oxygen relevant to the investigated system. The SEM-EDS results obtained for bimetallic catalysts confirmed the appearance of gold and copper at the same location in the case of bimetallic copper catalyst. The same result was obtained for gold–nickel supported catalyst or nickel at the same location. Furthermore, in the case of the bimetallic Au–Ni catalyst gold and nickel was observed in the same places on the MWCNTs surface. This result that the alloy formation is possible and this result agrees with the XRD and XPS data obtained for these catalysts.

3.7. The influence of metal addition on the acidity of multi-walled carbon nanotubes

Temperature-programmed desorption of ammonia is a conventional method for characterization ofthe acidity of catalytic materials [46]. TPD-NH_3 experiments were performed to elucidate the influence of Cu, Ni and Au on the acidity of prepared systems and to determine its effect on the catalytic reactivity in oxy-steam reforming of methanol reaction. TPD-NH_3 measurements were conducted over MWCNTs, mono- and bimetallic supported catalysts and the results are shown in Fig. 8. The distribution of acid centres was also calculated for all studied systems and the results are given in Table 2.

The acidity measurements showed that all samples exhibited three kinds of acid centres i.e., weak, medium and strong centres. The highest total acidity showed pristine MWCNTs material. Introduction of nickel or copper oxide into the nanomaterial resulted in decreasing of total acidity. The same effect was observed after metallic gold phase introduction to the monometallic supported

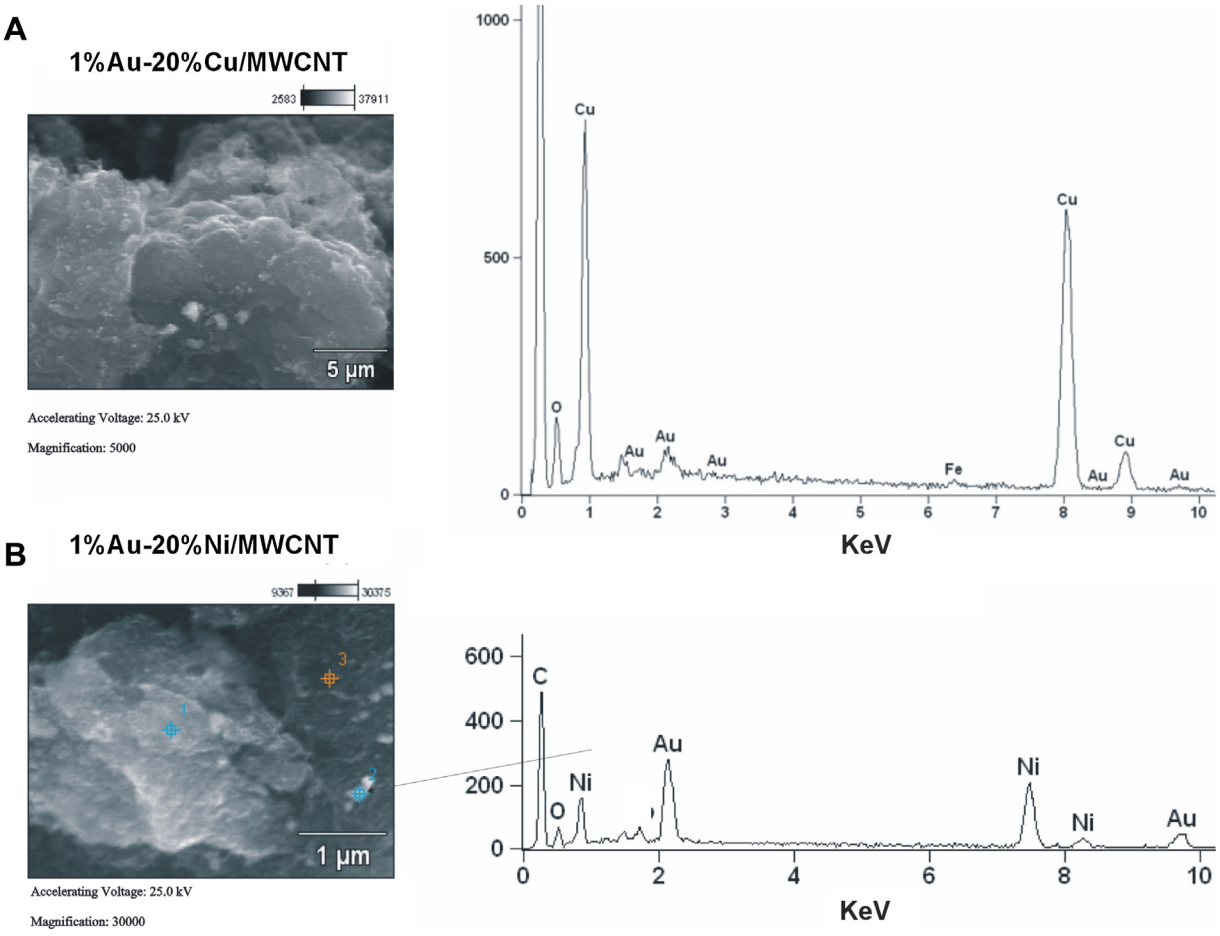

Fig. 7. SEM images of bimetallic (a) Au–Cu/MWCNTs and (b) Au–Ni/MWCNTs supported catalysts.

Table 2
The amount of NH_3 adsorbed on monometallic catalysts calcined in air atmosphere at 400 °C and on bimetallic catalysts calcined in air atmosphere at 180 °C calculated from the TPD-NH_3 data.

Catalysts	Weak centers [μmol/g] 100–300 °C	Medium centers [μmol/g] 300–450 °C	Strong centers [μmol/g] 450–600 °C	Total acidity [μmol/g] 100–600 °C
MWCNTs	143.7	42	652	837.7
20%Cu/MWCNTs	84	56	267.4	407.4
20%Ni/MWCNTs	31	70	429	530
1%Au–20%Cu/MWCNTs	35	21	676.4	732.4
1%Au–20%Ni/MWCNTs	51	87	263	401

catalysts. Different behavior was observed in the case of a copper catalyst promoted by gold. In this particular case the total acidity increased.

The acidity of functionalized MWCNTs and copper catalyst supported on MWCNTs was studied by Hareesh et al. [47]. The authors also observed three kinds of acid centers on the TPD-NH_3 profiles. It is well known from that NH_3 desorption peaks are in the range of 50–250 °C, 250–350 °C and above 350 °C and correspond to weak, moderate and strong acidic sites on the surface of the catalyst, respectively [47].

The acidic properties of MWCNTs containing system was also investigated by Ran et al. [48]. These workers studied pristine and functionalized MWCNTs obtained during the synthesis of the water assisted CVD method (MWCNTs-H_2O) and MWCNTs (MWCNTs-HNO_3) functionalized by acid treatment (HNO_3). The authors reported that the presence of the defects in the graphitic structure of MWCNTs may generate active sites for introduction of polar groups on their surface.

Temperature-programmed-desorption of ammonia was used to elucidate the difference in acidity of MWCNTs containing materials. The TPD-NH_3 results obtained for pristine MWCNTs showed a small and broad NH_3 desorption peak confirming the presence of few acidic groups which exist on the nanotube surface and are attributed to defects created in the MWCNTs during the synthesis process [16]. Analogous measurements were performed for MWCNTs-H_2O system. The results provide evidence that the same TPD effects were observed and characterized by higher intensity indicating greater amount of acidic sites, particularly weak acidic sites. Similar wide distribution of the acid sites was visible in the TPD curve recorded for MWCNTs-HNO_3. An important difference observed for this system was the appearance of a main desorption peak at higher temperature range (600–800 °C) indicating higher amount of strong acidic groups on the surface [16,48].

Table 3
Effect of temperature on the catalytic activity and selectivity to hydrogen, carbon monoxide and carbon dioxide in the oxy-steam reforming of methanol over mono- and bimetallic catalysts supported on MWCNTs.

Catalysts	CH_3OH conv. [%]		H_2 Selectivity [%]		CO Selectivity [%]		CO_2 Selectivity [%]	
	200 °C	300 °C	200 °C	300 °C	200 °C	300 °C	200 °C	300 °C
20%Cu/MWCNTs	11	75	38	63	0	8.5	62	28.5
20%Ni/MWCNTs	7.5	99.7	78.5	67.6	0	16.5	21.5	15.9
1%Au–20%Cu/MWCNTs	14	83	29.8	73	0	8.6	70.2	18.4
1%Au–20%Ni/MWCNTs	8	99.8	63.2	70.4	0	0	36.8	29.6

Reaction condition: weight of catalyst = 0.1 g, $H_2O/CH_3OH/O_2$ ratio in the feed = 1/1/0.4, temperature = 200 and 300 °C, atmospheric pressure, GHSV = 26700 h^{-1}.

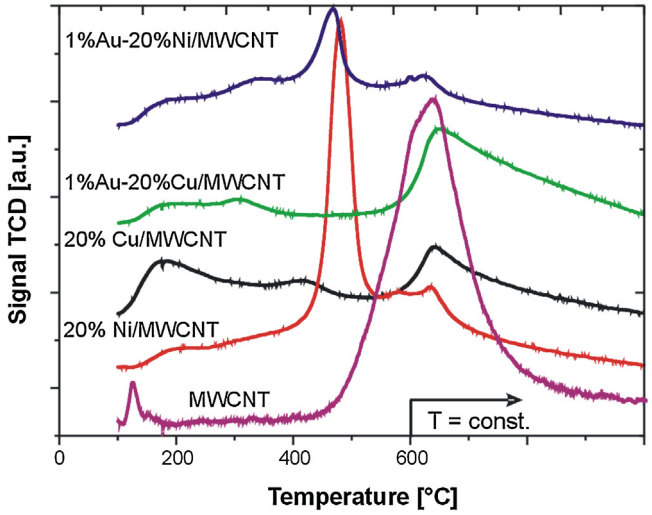

Fig. 8. TPD-NH_3 profile of multi-walled carbon nanotubes, mono- Cu, Ni catalysts after calcination in air for 4 h at 350 °C and bimetallic Au–Cu and Au–Ni catalysts after calcination in air for 4 h at 180 °C.

3.8. The influence of gold promotion on the catalytic activity and selectivity of the copper and nickel catalysts in oxy-steam reforming of methanol

The methanol oxy-steam reforming reactivity results for the mono (copper, nickel) and bimetallic Au–Cu and Au–Ni supported catalysts after reduction at 300 °C (copper containing catalysts) or 500 °C (nickel containing catalysts) in 5%H_2–95%Ar mixture are given in Table 3. The results from the methanol conversion in oxy-steam reforming of methanol showed that the reaction temperature increases for all catalytic systems. The activity results show that monometallic copper supported catalysts exhibited higher methanol conversion at 200 °C but lower at 300 °C compared to the nickel catalyst. In addition, promotion of copper catalysts by gold causes an increase in methanol conversion. Gold–nickel supported catalyst exhibited practically the same conversion of methanol at both temperature as monometallic nickel catalyst.

The selectivity results towards hydrogen, and carbon mono and dioxide formation are presented in the same Table 3. The results clearly show that the nickel catalysts exhibited higher selectivity to hydrogen in comparison to monometallic copper catalysts at the same temperature. Promotion of copper or nickel catalysts by gold causes increased selectivity towards hydrogen formation during the reaction carried out at 300 °C. Different results were obtained for bimetallic catalysts at 200 °C.

The selectivity values towards carbon monoxide and carbon dioxide formation are summarized in Table 3. For all systems, there was no formation of carbon monoxide at 200 °C. It is also worth noting that in the case of bimetallic Au–Ni catalyst carbon monoxide was not formed even at 300 °C. We did not observe the CO formation when the reaction carried out at 300 °C with bimetallic gold-nickel catalysts, but we have to remember that the concentration of CO was determined using TCD detector. The limit of detection of each compound by the TCD detector is in the range of 5–50 ng [49].

In the same table, the CO_2 selectivity results obtained for investigated system are also shown. The results confirm the promotion effect of gold on the selectivity of copper and nickel catalysts systems towards CO_2 formation. Decrease in selectivity to CO_2 at 300 °C was observed only in the case of Au–Cu systems. Furthermore, the high selectivity to carbon dioxide and hydrogen of the MWCNTs supported catalysts in oxy-steam reforming of methanol indicates that the main reaction which takes place during the process was oxy-steam reforming of methanol. The low carbon monoxide content indicates the reverse water gas shift reaction (RWGS) which runs to a limited extent [21].

Cu/ZnO-CNTs catalysts with various metal loading was tested in steam reforming of methanol (SRM) reaction in a fixed-bed reactor [21]. The activity results showed that the amount of hydrogen formed during the reaction increased with increasing of the reaction temperature and the main products in the studied reaction was hydrogen and carbon dioxide. The formation of a small amount of carbon monoxide was also observed. The same results were obtained in this work. The formation of CO_2, H_2 and CO confirmed that during the reaction only steam reforming of methanol and reverse water gas shift (RWGS) reaction took place. It was found that at a low reaction temperature, high metal loading catalysts exhibited higher methanol conversion, which was explained by the fact that SRM proceed easier [27].

In contrast to the reaction carried out at higher temperature both SRM and RWGS reactions proceed easier on catalysts with high metal loading which can explain greater CO formation [21,27].

The activity results obtained for the 23% wt.% Cu_{80}/ZnO_{20}-CNTs nano-catalysts showed that this system exhibited 88% and 95% methanol conversion at 280 and 320 °C, respectively. At the same time the selectivity to carbon monoxide was below 2% and selectivity to CO_2 above 20% at both temperatures. The same catalyst showed the selectivity to hydrogen formation of 63 and 72% at 280 and 320 °C, respectively. Based on above results we can summarize that our monometallic copper catalysts exhibited lower methanol conversion but similar H_2 and CO_2 selectivity at 300 °C. However, 20%Ni/MWCNTs systems showed highest selectivity to H_2 and lowest selectivity to CO formation in comparison to the both monometallic catalysts. In at the same time this system exhibited higher methanol conversion in the SRM reaction.

Mateos-Pedrero et al. [50] also studied various CuO/ZnO catalysts in steam refoming of methanol reaction at 220 and 300 °C in the conventional fixed bed reactor. They compared the reactivity results of those system with the commercial catalyst ($CuO/ZnO/Al_2O_3$ (66/24/10 wt.%) catalyst (G66-MR) supplied by Süd Chemie). The investigated catalysts exhibited conversion of methanol at 220 °C in the range of 7.9–15.9%, while industrial catalyst showed at the same temperature conversion of 63.8%. At a temperature of 300 °C various copper catalysts exhibited a conversion of methanol in the range of 64.2–82.2%, while the methanol conversion for the commercial catalyst was equal 90.1%.

The authors reported also that during the reaction carried out on various copper catalysts and commercial catalyst they observed the formation of CO in all cases as a by-product produced by endothermic reactions methanol decomposition (MD) and reverse water gas shift (RWGS) [5]. It is worth nothing that Ni/MWCNTs catalyst promoted by gold exhibited almost 100% of methanol conversion and during the reaction performed on this system CO was not formed, which makes that this system is important from the application point of view in fuel cell technology.

The activity results clearly confirm the promotion effect of gold on catalytic activity and selectivity of copper and nickel supported catalysts. The reactivity results are explained by the formation of Au–Cu or Au–Ni alloy formation during the activation process. The alloy Au–Cu and Au–Ni formation for the bimetallic catalytic systems was confirmed by XRD, XPS and SEM-EDS measurements.

The improvement in selectivity is associated with the surface modification of copper and nickel by gold atoms. These new gold atoms introduced into the structure of the alloy can generate new adsorption centres, which may be involved in the dissociative adsorption of methanol or adsorption of atomic oxygen as a result of dissociation of adsorbed methanol. Adsorbed oxygen atoms can leave the surface of the catalyst as a product of CO_2 thereby reducing the formation of CO, which can explain the lower bimetallic catalyst selectivity towards the formation of carbon monoxide.

Bimetallic Au–Cu/$Ce_{0.75}Zr_{0.25}O_2$ supported catalysts were prepared by a deposition–precipitation method and tested in steam reforming of methanol (SRM) in the range of 200–500 °C by Pojanavaraphan et al. [51]. Upon completion of the activity measurements over series of catalysts, the authors found that the variation of Au/Cu composition significantly affected on the catalytic activity of SRM. The activity results, as in the case of our reaction, showed that methanol conversion, the yield of hydrogen and selectivity increase with reaction temperature consistent with an endothermic reaction. However, they claimed that the bimetallic catalysts systems were not as active compared to the monometallic catalysts. In addition, differences in CO selectivity were not observed for the catalysts below 400 °C. Only a slight difference in hydrogen formation was observed for all catalytic materials.

4. Conclusions

This work provides evidence of Au–Cu or Au–Ni alloy formation in the case of bimetallic Au–Cu/MWCNTs and Au–Ni/MWCNTs catalyst after their reduction at 300 °C and 500 °C in mixture of 5%H_2–95%Ar, respectively. During bimetallic catalysts reduction carried out at 300 °C the Au–Cu and Au–Ni alloy formation was demonstrated by XRD, XPS and SEM-EDS measurements. The spillover effect between metallic gold and nickel oxide was confirmed by reduction studies performed for Au–Ni/MWCNTs catalysts. The same effect was observed for the bimetallic catalysts Au–Cu/MWCNTs. There was a significant improvement in the catalytic activity and selectivity to hydrogen formation of bimetallic Au–Cu catalysts compared to monometallic systems in OSRM reaction at 300 °C. The higher activity and selectivity to hydrogen of the bimetallic gold–copper supported catalysts can be attributed by the alloy compound formation. The lowest selectivity towards CO formation both at 200 and 300 °C was detected for bimetallic Au–Ni/MWCNTs catalyst, which is very important from the practical point of view. The facilitation of the oxidation of multi-walled carbon nanotubes after addition of metal oxide and the stability of the prepared system under the reaction conditions was proven by TG measurements. The TPD -NH_3 measurements confirmed the occurrence of three kinds of acid centers, which correspond to weak, moderate and strong acidic sites on the catalyst surface.

Acknowledgement

The project was funded by the National Science Centre (Grant no. DEC-2012/05/D/ST8/02856).

Appendix A. Supplementary data

Supplementary data associated with this article can be found, in the online version, at http://dx.doi.org/10.1016/j.apcatb.2015.11.047.

References

[1] P. López, G. Mondragón-Galicia, M.E. Espinosa-Pesqueira, D. Mendoza-Anaya, M.E. Fernández, A. Gómez-Cortés, J. Bonifacio, G. Martínez-Barrera, R. Pérez-Hernández, Int. J. Hydrogen Energy 37 (2012) 9018–9027.
[2] P. Mierczynski, K. Vasilev, A. Mierczynska, W. Maniukiewicz, T. Maniecki, Top. Catal. 56 (2013) 1015–1025.
[3] P. Mierczynski, K. Vasilev, A. Mierczynska, W. Maniukiewicz, T.P. Maniecki, Appl. Catal. A 479 (2014) 26–34.
[4] R. Pérez-Hernández, A. Gutiérrez-Martínez, M.E. Espinosa-Pesqueira, M.L. Estanislao, J. Palacios, Catal. Today 250 (2015) 166–172.
[5] S. Sá, H. Silva, L. Brandão, J.M. Sousa, A. Mendes, Appl. Catal. B 99 (2010) 43–57.
[6] R. Pérez-Hernández, G. Mondragón Galicia, D. Mendoza Anaya, J. Palacios, C. Angeles-Chavez, J. Arenas-Alatorre, Int. J. Hydrogen Energy 33 (2008) 4569–4576.
[7] R. Pérez-Hernández, A. Gutiérrez-Martínez, J. Palacios, M. Vega-Hernández, V. Rodríguez-Lugo, Int. J. Hydrogen Energy 36 (2011) 6601–6608.
[8] L.F. Bobadilla, S. Palma, S. Ivanova, M.I. Domínguez, F. Romero-Sarria, M.A. Centeno, J.A. Odriozola, Int. J. Hydrogen Energy 38 (2013) 6646–6656.
[9] P. Mierczynski, T. Maniecki, W. Maniukiewicz, W. Jozwiak, React. Kinet. Mech. Catal. 104 (2011) 139–148.
[10] T. Maniecki, K. Bawolak, P. Mierczynski, W. Jozwiak, Catal. Lett. 128 (2009) 401–404.
[11] T. Maniecki, K. Bawolak-Olczak, P. Mierczynski, W. Maniukiewicz, W. Jozwiak, Chem. Eng. J. 154 (2009) 142–148.
[12] A. Sandoval, C. Louis, R. Zanella, Appl. Catal. B 140–141 (2013) 363–377.
[13] T. Maniecki, P. Mierczynski, W. Maniukiewicz, K. Bawolak, D. Gebauer, W. Jozwiak, Catal. Lett. 130 (2009) 481–488.
[14] V. Dal Santo, A. Gallo, A. Naldoni, M. Guidotti, R. Psaro, Catal. Today 197 (2012) 190–205.
[15] G. Chen, S. Li, Q. Yuan, Catal. Today 120 (2007) 63–70.
[16] P. Serp, M. Corrias, P. Kalck, Appl. Catal. A 253 (2003) 337–358.
[17] L. Yang, G.-D. Lin, H.-B. Zhang, Appl. Catal. A 455 (2013) 137–144.
[18] R. Barthos, F. Solymosi, J. Catal. 249 (2007) 289–299.
[19] P. Sangeetha, L.-H. Chang, Y.-W. Chen, Mater. Chem. Phys. 118 (2009) 181–186.
[20] A. Mahajan, A. Kingon, Á. Kukovecz, Z. Konya, P.M. Vilarinho, Mater. Lett. 90 (2013) 165–168.
[21] H.-M. Yang, P.-H. Liao, Appl. Catal. A 317 (2007) 226–233.
[22] R.M.M. Abbaslou, A. Tavassoli, J. Soltan, A.K. Dalai, Appl. Catal. A 367 (2009) 47–52.
[23] C. Baatz, N. Decker, U. Prüße, J. Catal. 258 (2008) 165–169.
[24] W.K. Jóźwiak, T.P. Maniecki, Thermochim. Acta 435 (2005) 151–161.
[25] J. Zhang, J.-O. Müller, W. Zheng, D. Wang, D. Su, R. Schlögl, Nano Lett. 8 (2008) 2738–2743.
[26] H.S. Zeng, K. Inazu, K.-i. Aika, Appl. Catal. A 219 (2001) 235–247.
[27] P. Mierczynski, R. Ciesielski, A. Kedziora, M. Nowosielska, J. Kubicki, W. Maniukiewicz, A. Czylkowska, T.P. Maniecki, React. Kinet. Mech. Catal. (2015) 1–17.
[28] T. Maniecki, P. Mierczynski, W. Jozwiak, Kinet. Catal. 51 (2010) 843–848.
[29] T. Maniecki, P. Mierczynski, W. Maniukiewicz, D. Gebauer, W. Jozwiak, Kinet. Catal. 50 (2009) 228–234.
[30] Z. Liu, M.D. Amiridis, Y. Chen, J. Phys. Chem. B 109 (2005) 1251–1255.
[31] M. Turco, G. Bagnasco, C. Cammarano, P. Senese, U. Costantino, M. Sisani, Appl. Catal. B 77 (2007) 46–57.
[32] S. Song, S. Jiang, Appl. Catal. B 117–118 (2012) 346–350.
[33] A.K. Chakraborty, R.A.J. Woolley, Y.V. Butenko, V.R. Dhanak, L. Šiller, M.R.C. Hunt, Carbon 45 (2007) 2744–2750.
[34] T. Maniecki, A. Stadnichenko, W. Maniukiewicz, K. Bawolak, P. Mierczynski, A. Boronin, W. Jozwiak, Kinet. Catal. 51 (2010) 573–578.
[35] M. Zhou, L. Tian, L. Niu, C. Li, G. Xiao, R. Xiao, Fuel Process. Technol. 126 (2014) 12–18.
[36] Handbook of Copper Compounds and Applications, in: H.W. Richardson (Ed.), Marcel Dekker Inc., New York, NY, U.S.A, 1997, p. 71.
[37] O. Mabayoje, M. Seredych, T.J. Bandosz, ACS Appl. Mater. Interfaces 4 (2012) 3316.
[38] C.-X. Sun, Y. Wang, A.-P. Jia, S.-X. Chen, M.-F. Luo, J.-Q. Lu, J. Catal. 312 (2014) 139–151.
[39] H. Pasupulety, Y.A. Driss, A.A. Alhamed, M.A. Alzahrani, Appl. Catal. A. (2015).
[40] C. Kartusch, J. van Bokhoven, Gold Bull. 42 (2009) 343–348.

[41] H. Wu, G. Pantaleo, V. La Parola, A.M. Venezia, X. Collard, C. Aprile, L.F. Liotta, Appl. Catal. B 156–157 (2014) 350–361.
[42] A. Horváth, L. Guczi, A. Kocsonya, G. Sáfrán, V. La Parola, L.F. Liotta, G. Pantaleo, A.M. Venezia, Appl. Catal. A 468 (2013) 250–259.
[43] C.-Y. Lu, H.-H. Tseng, M.-Y. Wey, T.-W. Hsueh, Chem. Eng. J. 145 (2009) 461–467.
[44] P. Steiner, S. Hüfner, Solid State Commun. 37 (1981) 279–283.
[45] F. Yang, Y. Yao, Z. Yan, H. Min, D.W. Goodman, Appl. Surf. Sci. 283 (2013) 263–268.
[46] P. Mierczynski, K.A. Chalupka, W. Maniukiewicz, J. Kubicki, M.I. Szynkowska, T.P. Maniecki, Appl. Catal. B 164 (2015) 176–183.
[47] H.N. Hareesh, K.U. Minchitha, N. Nagaraju, N. Kathyayini, Chin. J. Catal. 36 (2015) 1825–1836.
[48] M. Ran, W. Sun, Y. Liu, W. Chu, C. Jiang, J. Solid State Chem. 197 (2013) 517–522.
[49] J. Cazes, Encyclopedia of Chromatography, 2nd ed., Published by Taylor & Francis Group, 6000 Broken Sound Parkway NW, Suite 300 BocaRaton, 2006.
[50] C. Mateos-Pedrero, H. Silva, D.A. Pacheco Tanaka, S. Liguori, A. Iulianelli, A. Basile, A. Mendes, Appl. Catal. B 174–175 (2015) 67–76.
[51] C. Pojanavaraphan, A. Luengnaruemitchai, E. Gulari, Appl. Catal. A 456 (2013) 135–143.